sustainability

MDPI

Article

Effect of Different Activators on Properties of Slag-Gold Tailings-Red Mud Ternary Composite

Haonan Cui [1,*], Haili Cheng [1], Tianyong Huang [2], Feihua Yang [2], Haoxiang Lan [2] and Jvlun Li [2]

[1] School of Civil Engineering, North China University of Technology, Beijing 100144, China
[2] Beijing Building Materials Academy of Sciences Research, Beijing 100041, China
* Correspondence: 15689713762@163.com

Abstract: Red mud is a kind of solid waste produced in the process of aluminum extraction. Traditional methods of red mud treatment, such as open-pit accumulation and chemical recovery, are costly and environmentally hazardous. Gold tailings are industrial by-products produced in the process of gold mining and refining. In this study, NaOH, KOH, and Na_2SiO_3 were used as activators, and their effects on the properties of ternary cementitious composite containing blast furnace's slag, gold tailings, and red mud were studied with the intention of preparing a new cementitious material that is an efficient recovery and utilization of solid waste. The macroscopic mechanical properties and hydration of the ternary cementation material were studied by means of compressive strength, XRD, FT-IR, and TG/DTG. The compressive strength testing showed that the maximum strength at 28 d was 43.5 MPa. The hydration products in the ternary cementitious system were studied by SEM and EDS, and it has been demonstrated that the strength of this cement was due to the formation of Aft (AFt, also known as Ettringite, has the chemical formula $3CaO{\cdot}Al_2O_3{\cdot}3CaSO_4{\cdot}32H_2O$. It is one of the important hydration products of cement-based cementitious materials, which can not only provide early strength for cement, but also compensate for early shrinkage of concrete.) and C-A-S-H gels. Samples activated by Na_2SiO_3 presented a most compact microstructure and the best macroscopic mechanical properties than the samples free of activator. The toxicity tests results showed that the content of heavy metal ions liberated by the cement's leaching met the standard requirements, proving that the slag-gold tailings-red mud ternary composite was environmentally friendly.

Keywords: red mud; gold tailings; geopolymer; solid waste utilization; cementitious materials

check for updates

Citation: Cui, H.; Cheng, H.; Huang, T.; Yang, F.; Lan, H.; Li, J. Effect of Different Activators on Properties of Slag-Gold Tailings-Red Mud Ternary Composite. *Sustainability* **2022**, *14*, 13573. https://doi.org/10.3390/su142013573

Academic Editor: Ning Yuan

Received: 12 September 2022
Accepted: 12 October 2022
Published: 20 October 2022

Publisher's Note: MDPI stays neutral with regard to jurisdictional claims in published maps and institutional affiliations.

Copyright: © 2022 by the authors. Licensee MDPI, Basel, Switzerland. This article is an open access article distributed under the terms and conditions of the Creative Commons Attribution (CC BY) license (https://creativecommons.org/licenses/by/4.0/).

1. Introduction

In 2020, about 3.787 billion tons of bulk solid waste were produced in China, of which about 3.1 billion tons were hazardous, with a utilization rate estimated at only 48.67% [1]. Improving the comprehensive utilization level of hazardous solid waste is of great significance to the construction of waste free city and the recycling of renewable resources.

Red mud (RM) is one of the main solid wastes generated by the process of aluminum extraction from bauxite [1]. Producing 1 ton of alumina produces about 1 to 1.5 tons of red mud, and about 250 million tons of red mud are produced every year worldwide [2]. In 2020, China produced 106 million tons of red mud with the comprehensive utilization rate of only 7.05% [3], that is, a value far below far below the world averaged value. Indeed, 90% of the red muds produced by the global electrolytic aluminum industry is Bayer red mud [4]. This mud presents higher basicity and heavy metal content, limiting its utilization rate as resource [5]. Therefore, green development and utilization of red mud is urgent for minimizing the pollution of soil and groundwater. The authors of [6,7] investigated the effect of red mud as a mineral additive to substitute cement in the construction of concrete, that is, on its performance and application in regular manufacturing. Indeed, when the amount of red mud is 10 percent by weight, the mechanical properties of concrete are unaffected. The addition of red mud can increase the sulfate resistance of concrete.

The authors of [8] investigated the impact of red mud on the working and mechanical properties of concrete and observed that the addition of red mud had no effect on the hydration process. The mechanical strength, however, declines as the red mud component approaches 20% by weight. Similar results were reported by [9,10], respectively.

In the process of gold production and processing, considerable industrial by-products called gold tailings (GT) are produced [11]. China produced 188 million tons of gold tailings in 2020, with a comprehensive utilization rate of less than 20 percent. The main reason behind is that gold tailings after cyanidation still contain harmful substances, such as cyanide and heavy metal ions of Cd, Ni, Zn, and Pb [12,13]. Open-pit accumulation causes harmful substances release from gold tailings to the soil and change soil composition, thus damaging the environment for plant growth [14]. Therefore, a new means of disposing of gold tailings must be identified. The authors of [15] examined the effect of gold tailings substituting ordinary Portland cement (OPC), and discovered that the GT-OPC mixture met the minimum compressive strength standards for road construction. The author of [16]. studied the effect of gold tailings mixed into sulfoaluminate cement on mechanical characteristics and hydration effect. They noticed that such cement possessed superior mechanical qualities and excellent sulfate curing capacity.

In previous studies, red mud and gold tailings were traditionally added directly to cement to replace a portion of cement [17]. Although this seemed a best choice for waste solid disposal, Portland cement production was often accompanied by great carbon dioxide emissions, high energy consumption with high pollution, and waste [18]. Therefore, alternative materials with good mechanical properties that can be produced at room temperature, and without the release of secondary harmful substances, it becomes more and more attractive [19,20]. Using geopolymer materials as a substitute for traditional building materials stands for best alternative. Red mud, gold tailings, and slag with high aluminum silicate content are good raw materials for the preparation of geological polymer, that can be used, after activation, to replace traditional Portland cement concrete [21]. This not only reduces the exploitation of natural minerals but also achieves a "carbon neutral" goal [22]. Byproducts from the production of blast furnace iron are utilized to make cementitious materials because they are of high pozzolanic activity. Geopolymers can be also made from slag, and are viewed as an excellent secondary raw material [23,24].

Few studies have been done on how to prepare geopolymers using solid waste-made cementing materials composed of red mud, gold tailings, and mineral powder. Most of the research focuses on using alkali activated tailings as filling materials [16,25–27]. Furthermore, in most studies, only specific solid waste is used to develop geopolymers so that the combined use of red mud and gold tailings to produce alkali-activated cementing materials has not yet been reported [28]. This research investigates effects from NaOH, KOH, and Na_2SiO_3 (modulus = 1) as activators on the mechanics and hydration products, and evaluates microstructure of the ternary composite system, that is, slag-gold tailing-red mud made cementitious material (SGRCM). This material can not only help minimize environmental pollution from red mud and gold tailings, but also reduce the construction cost. Given that red mud, one of the raw materials, has a huge similarity to that of a sintered red brick, it may be used as a pigment to obtain red-colored mud bricks, colored pavements, colored concretes, and other decorative products. The prepared products do not need pigments or secondary coloring, directly in line with the requirements of architectural aesthetics. From a global perspective, the development of SGRCM will favor an efficient utilization of solid waste and reducing the dependence of the construction industry on traditional Portland cement.

2. Materials and Methods

2.1. Materials and Reagents

The red mud used to prepare SGRCM was provided by an aluminum plant in Shandong Province, China. Slag was supplied from a steel mill in Beijing, China. Gold tailings were sourced from a gold mining company in Yantai, China. Building plaster (BP) was

purchased from the market. The reagents used in this test were: 99.9% purity sodium hydroxide, potassium hydroxide, and fine granular sodium silicate (modulus = 1). The main chemical elements of red mud, slag, and gold tailings were determined by X-ray fluorescence spectrometer (XRF), with the results shown in Table 1. Correspondingly, Table 1 also gives the loss on ignition (L.O.I.) of the raw materials. The total alkali content in the raw materials is also counted in Table 1. To more intuitively reflect the alkali concentration of the raw material, the size of the alkali concentration in the raw material is expressed by the pH value. The instrument for testing PH is PE20K laboratory PH machine, and the results are also shown at the end of Table 1. The particle size distributions of red mud, gold tailings, and slag were measured by a MS2000 laser particle size analyzer (see Figure 1) as shown in Figure 1. The size distribution of red mud was significantly smaller than that of slag and gold tailings. The radioactivity of red mud and gold tailings was determined using internal exposure index (the ratio of the specific activity of radionuclide radium-226 in the material to the limit specified in the standard) and external exposure index (the sum of the ratio of the specific activity of radionuclide radium-226, thorium 232, and potassium 40 in the material to the limit specified in the standard). The obtained results are shown in Table 2. XRD patterns of red mud, gold tailings, and slag are shown in Figure 2. XRD Quartz and feldspar ate the main mineral components of gold tailings while the red mud contains a hematite and amorphous silicoaluminate phase. As for the slag, it is mainly composed of amorphous glass phase.

Table 1. Raw materials chemical composition, loss on ignition (wt.%), and PH.

Material	SiO_2	Fe_2O_3	Al_2O_3	CaO	Na_2O	TiO_2	K_2O	SO_3	MgO	Others	Total Alkalinity	L.O.I.	PH
Red mud	22.91	22.13	18.15	3.64	9.39	3.50	0.96	0.84	0.83	0.68	7.73	5.12	10.55
Slag	28.02	0.78	16.42	37.37	-	2.51	0.50	1.80	10.04	3.76	-	0.09	10.82
Gold tailings	61.44	2.44	18.33	2.47	2.85	0.25	5.31	1.31	0.85	0.56	5.84	3.58	8.97

2.2. Test Contents and Methods

2.2.1. Sample Preparation

The cementitious material (SGRCM) is composed of red mud (10%), gold tailings (40%), slag (45%), and construction gypsum (5%). The effects of activators on the properties of the SGRCM were studied based on the mixture ratio. The amount of the added activator was set at 2 wt.%. The Chinese national standard GB/T 17671-2021 is referred to as the preparation of paste samples. The specific method is to mix the solid powder and the alkali solution mixed with different activators, pour it into a planetary mixer, and stir for 5 min. Subsequently, the slurry was uniformly cast in a steel mold with dimensions of 40 mm × 40 mm × 160 mm, cured at a temperature of 20 ± 1 °C, and had a relative humidity of 90%. The sample prepared without the activator was named SGRCM0, whereas those containing NaOH, KOH, and Na_2SiO_3 as activators were named SGRCM1, SGRCM2, and SGRCM3, respectively (see Table 3). The water-binder ratio used during the experiment (at room temperature) was set at 0.5.

2.2.2. Strength Test

Standard mortar samples with size of 40 × 40 × 160 mm were prepared according to GB/T17671-2021. The samples were cured for 3, 7, and 28 days at humidity ≥95% and temperature 20 ± 1 °C, respectively. When reaching the age, the whY-3000 pressure tester is used to test the bending strength and compressive strength of the sample. At the same time, there was a batch of 20 mm × 20 mm × 20 mm neat cement blocks, which were maintained under the same environment. The samples were taken out at 3, 7, and 28 days, respectively, and the hydration was terminated with isopropyl alcohol for microscopic analysis.

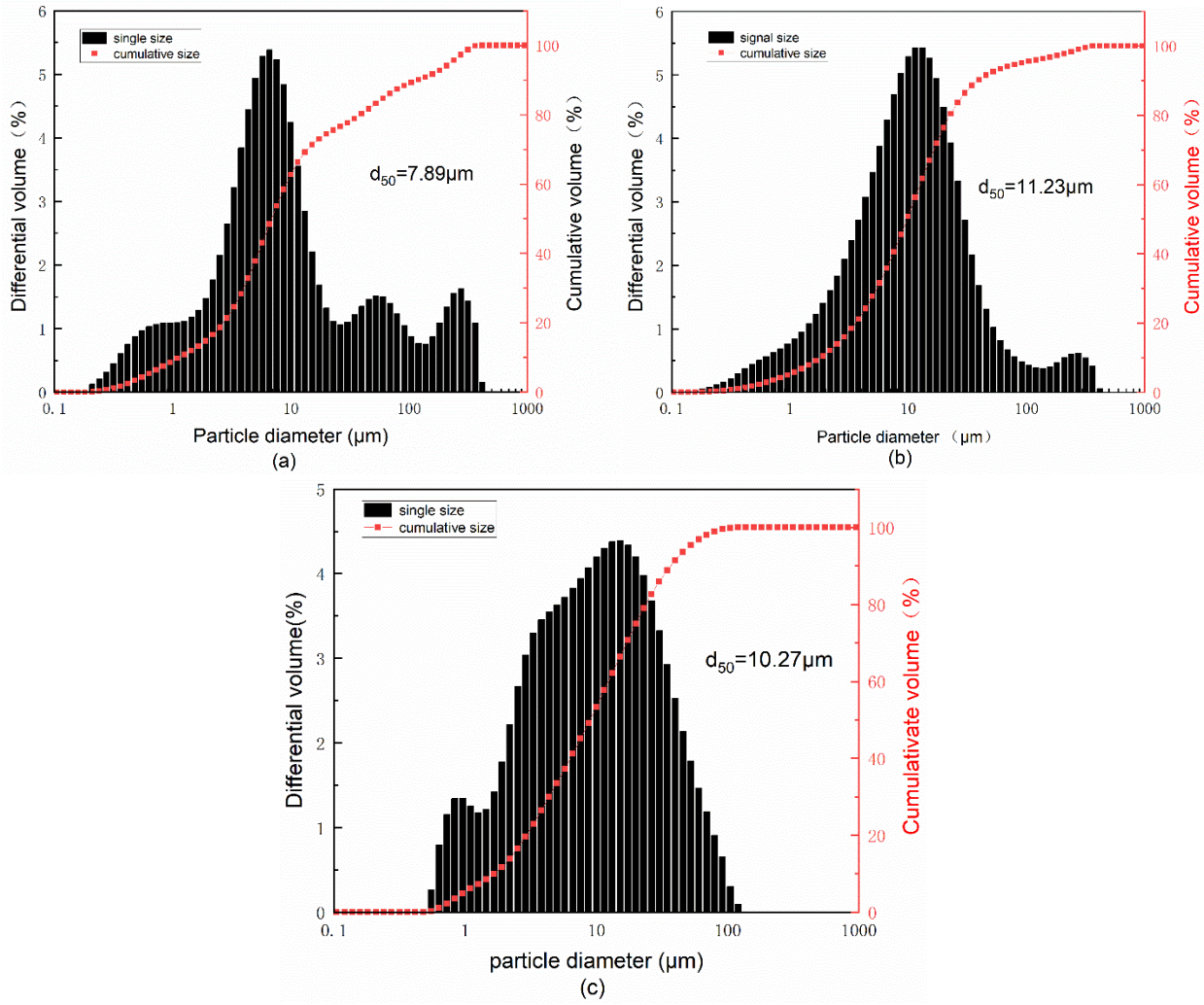


Figure 1. Particle diameter distribution of (**a**) red mud, (**b**) slag, and (**c**) gold tailings.

Table 2. Raw materials radioactivity.

Material	Internal Exposure Index	External Exposure Index
Red mud	1.83	1.78
Waste gold tailing	0.15	0.67

2.2.3. XRD Analysis

The samples were analyzed using an X-ray diffrotometer (Rigaku Corporation, Ultima IV, Tokyo, Japan), X-ray tube type: Cu target (maximum output power: 2 kW), and scanning method: THERA/2THERA Goniometer, with the samples being stationary.

2.2.4. Infrared Spectral Analysis

1 mg sample was mixed with spectrographic-graded KBr (100 mg) and homogeneously grinded. An infrared spectrometer model, iS10 (NICOLET), was used, in spectral range of 7800–350 cm^{-1}, with linear accuracy better than 0.1%.

2.2.5. Thermogravimetric Analysis

The instrument used for thermogravimetric (TG) analysis was SDT Q600 with a temperature range of 30 to 1000 °C and a heating rate of 20 °C/min in a nitrogen environment.

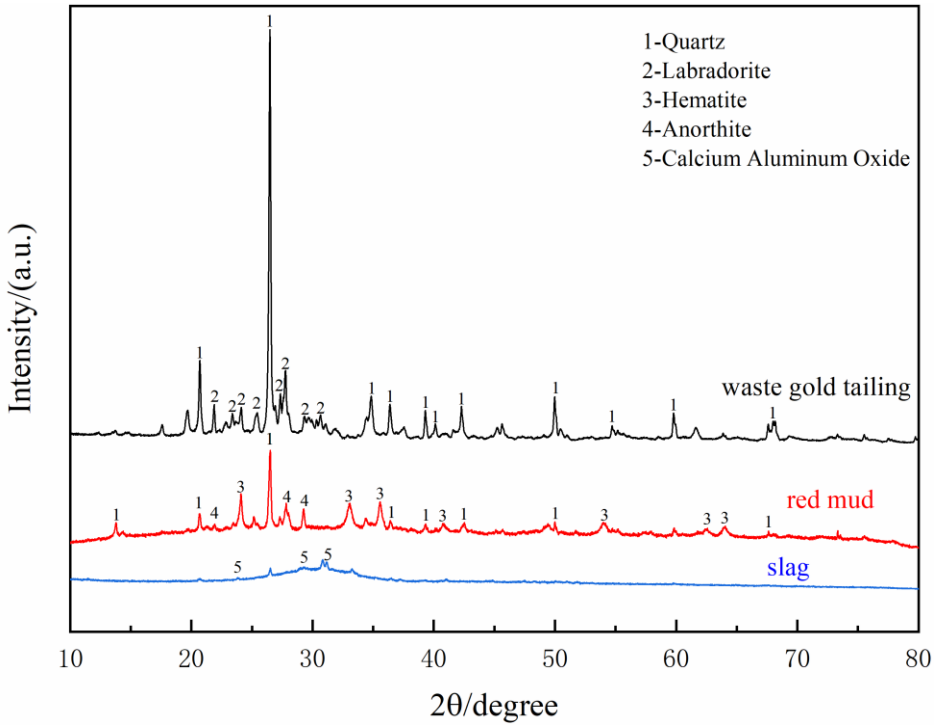


Figure 2. X-ray diffraction spectra of waste gold tailing, red mud, and slag.

Table 3. Mixing proportion of samples, wt.%.

Samples	NaOH	KOH	Na_2SiO_3	Building Plaster	Slag	GT	RM
SGRCM0	-	-	-	5	45	40	10
SGRCM1	2	-	-				
SGRCM2	-	2	-				5
SGRCM3	-	-	2				

2.2.6. Microscopic Morphology Analysis

The microscopic morphology analysis of SGRCM was taken by s-3400 N electron microscope (manufacturer: Hitachi, Marunouchi, Japan) at 20 kV. The interfaces of the different samples are knocked out, the samples are fixed to the SEM sample holder with conductive tape, and they are then sprayed with a thin layer of gold to improve electrical conductivity.

2.2.7. Leachability Test

Due to the complexity of the raw materials used to prepare SGRCM, it is necessary to evaluate the environmental impact of SGRCM. In this study, the leaching toxicity of SGRCM using different activators was conducted according to HJ/T299, 2007 standard method. The 10 g sample was crushed into particles with a diameter of smaller than 9.5 mm and mixed with 100 mL sulfuric acid/nitric acid (mass ratio M (H_2SO_4): M (HNO_3) was 2:1), with the pH set at 3.20 ± 0.05. After the sample was mixed with the leaching solution, the bottle was enclosed and fixed on the rotating oscillation device, with the speed adjusted to 30 ± 2 r/min, and the oscillation achieved at 23 ± 2 °C for 18 ± 2 h. The filter membrane was installed on the pressure filter, rinsed with dilute nitric acid, and the leaching solution was filtered with the filtrate collected by the inductively coupled plasma mass spectrometer (Model NexION 300X) in view chemical analysis.

3. Results and Discussion

3.1. Compressive Strength Analysis

The flexural strength and compressive strength of SGRCM prepared without activator (controlled samples) and samples containing 2 wt.% NaOH, KOH and Na_2SiO_3 have been measured according to the specification GB/T17671-2021 as shown by the results depicted in Figure 3. The addition of NaOH and KOH decreased the samples strength compared to that of the control sample. This is due to the fact that the red mud, gold tailings, and slag are alkaline materials, so they had brought too much OH^- chemical species. This resulted in increased internal alkalinity and in a speeded precipitation of hydration products on the surface of glassy particles inhibiting their hydration reaction. The addition of Na_2SiO_3 did not contribute to sample early strength and after 7 d, the compressive strength was improved with the increase of curing time. At 7 d, the compressive strength was 30.41% higher than the value given the control sample and has reached 34.43 MPa. This revealed that the sample activated using Na_2SiO_3 displayed a better mechanical performance when compared to other samples. Moreover, Na_2SiO_3 itself has adhesive properties capable of improving the strength of the sample at an early stage.

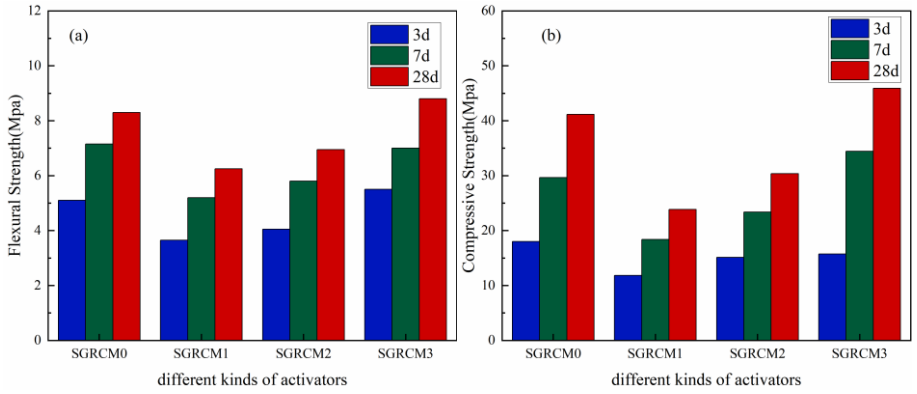


Figure 3. Effects of different activators on flexural strength (**a**) and compressive strength (**b**).

3.2. XRD Analysis

To determine the mineral phase' s composition of hydration products, XRD analysis was performed on SGRCM blocks prepared with different activators, and were analyzed by XRD after different curing ages (3, 7, 28 d), as shown in Figure 4. Figure 4A presents the X-ray diffraction patterns of SGRCM prepared without the activator after 3, 7, and 28 days. As for Figure 4B–D show the XRD patterns of SGRCM activated by NaOH, KOH, and Na_2SiO_3 (modulus = 1). Figure 4A–D reveals that after 28 d, ettringite (AFt), mullite, and anorthite ($2CaO{\cdot}Al_2O_3{\cdot}SiO_2$) are the primary hydration products [29]. Ettringite consists of crystallized hydrated calcium sulfoaluminate produced by the hydration reaction involving calcium aluminates and sulfate ion. This indicates that the hydration products formed by the active aluminates in the raw materials were the main source of strength shown by SGRCM.

Residual quartz was also found in the raw material. It may cause micro aggregate reaction, that is, a positive effect on improving strength. In addition, the diffraction peaks of ettringite and mullite were seen at 3 d in samples prepared without an activator, but those peaks are much weaker in samples prepared with NaOH and KOH as activator. This indicates that the addition of NaOH and KOH has inhibited the formation of ettringite. The alkalinity provided by red mud, gold tailings, and ore powder (red mud pH = 10.55, gold tailings pH = 8.79, slag pH = 10.82) was sufficient for converting glassy phases in ore powder into C-A-S-H. However, after the addition of alkali, pH was so high that the C-A-S-H gels generated quickly precipitated on the glass phase surface [30,31]. Consequently, the glass phase failed to contact the alkali solution, so the hydration reaction is inhibited [32,33].

On the contrary, the addition of Na_2SiO_3 resulted in a slight pH change, therefore the introduced silicon promoted the hydration reaction [34].

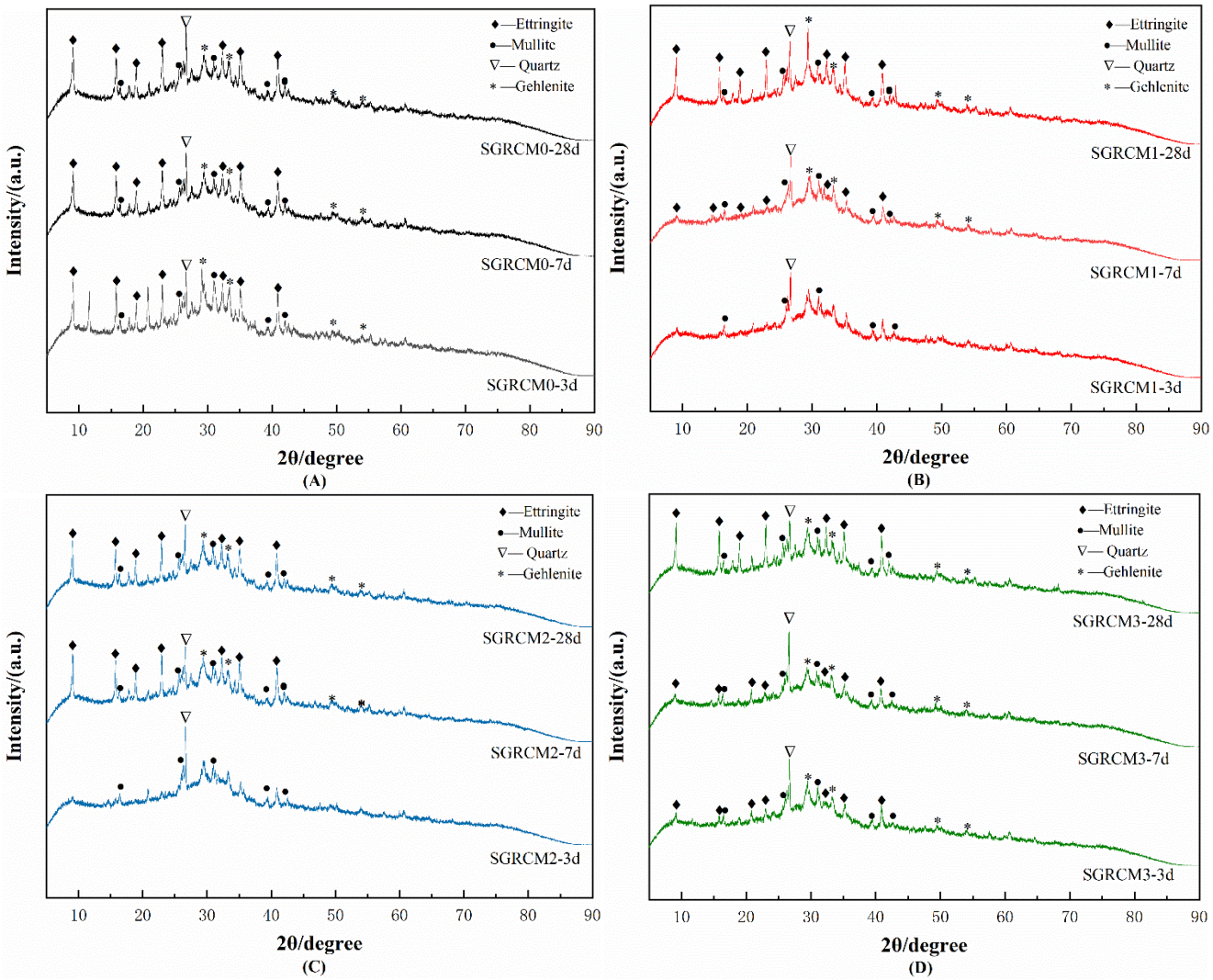


Figure 4. XRD spectrum of the SGRCM cured for 3 d/7 d/28 d with different activators. (**A**) shows the XRD plots of SGRCM at 3, 7, and 28 d without the addition of an activator. (**B**–**D**) are the XRD plots at 3, 7, and 28 d when NaOH, KOH, and Na_2SiO_3 were added as the activator.

3.3. FT-IR Spectroscopy Analysis

Figure 5 depicts the FT-IR spectra of SGRCM at 3 d and 28 d. It can be seen that the FT-IR spectra of samples prepared with or without activators look basically the same. The absorption peak seen at 3430 cm^{-1} stands for asymmetric stretching vibration of hydroxyl (X-OH) [35]. As for the absorption peak seen at 1630 cm^{-1}, it is associated with the bending vibration of H-O-H in C-A-S-H [27]. Under the combined activation of red mud, gold tailings and gypsum, SGRCM produced numerous hydrates (products containing water). In Figure 4, there is a weak absorption peak at 3150 cm^{-1}, which is caused by the stretching vibration of OH^-. The strong absorption peak at 1090 cm^{-1} is caused by the asymmetric stretching vibration of SO_4^{2-} in AFt. This reveals that ettringite can be generated in both the early stage and the late stage regardless of the activator used. It is clear that the ettringite crystals are involved in the early strength of SGRCM. The results are consistent with those from XRD and SEM analyses. In addition, the absorption peak at 1440 cm^{-1} is caused by CO_3^{2-} antisymmetric stretching vibration due to carbonization of samples exposed to air. There are also two absorption peaks between 400 cm^{-1} and 1000 cm^{-1}, associated to the

tensile and angular bending vibration of Si-O-Al and Si-O-Si bonds [36]. This indicates the presence of silicaluminate groups in the geopolymer structure, similar to the hydrated calcium silicaluminate (C-A-S-H) formed during cement hydration. The FTIR spectra of different SGRCM activated using different activators did not show any obvious difference. This reveals the fact that different activators do not reduce the formation of aluminosilicate gel, but only change the intensity of the band associated with the Si and Al bonds.

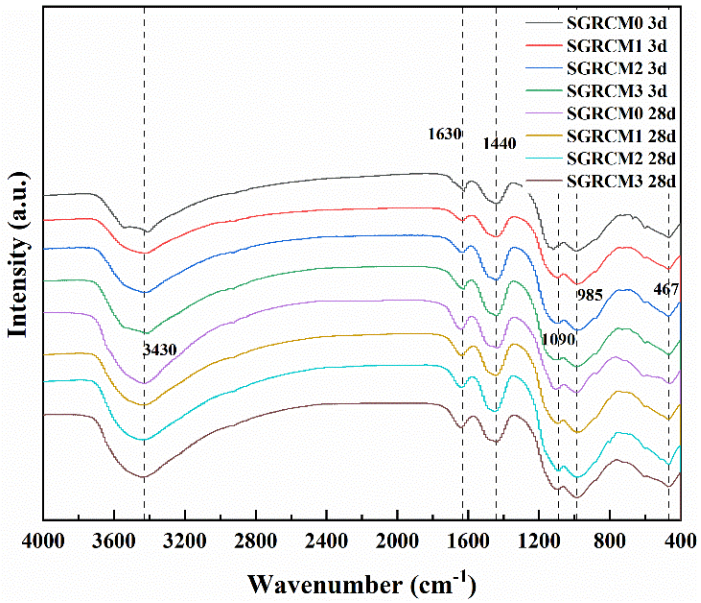


Figure 5. Geopolymer patterns produced by FTIR.

3.4. Thermogravimetric Analysis

The thermogravimetric and differential heat curves of SGRCM hardened slurry at 1 d and 28 d are shown in Figure 6. As can be seen from the figure, there are three weight loss intervals for all samples, and 28 d samples have greater weight loss in each interval than the 1 d samples. The first weight loss interval was 50–250 °C, with two endothermal peaks at 100 °C and 150 °C on the DTG curve, respectively. The peak at 100 °C was caused by the loss of crystallization water from hydration product AFt and the loss of interlayer water of C-A-S-H gel [11]. The peak at 150 °C has probably been caused by the dehydration of gypsum into hemihydrate gypsum. By comparing the DTG curves at 28 d and 3 d, it can be seen that the two peaks at 100 °C and 150 °C at 3 d emerge as the ones seen at about 100 °C after 28 d. The peak become wider and sharper obviously. given that the content of C-A-S-H gel and AFt has increased with the extension of curing age [37]. After 28 d, the peak at 150 °C disappeared, showing that gypsum was gradually and completely consumed with the increase of hydration age. The peak at 450 °C in the DTG curves of samples cured for 1 d and 28 d demonstrates the presence of Ca $(OH)_2$. of which the peak weakened after 28 d due to the continuous consumption of Ca $(OH)_2$ by the pozzolanic reactions. For samples cured for 3 d and 28 d, a peak was also seen at 600–800 °C are also found. This peak stands for the $CaCO_3$ produced through carbonation of Ca $(OH)_2$ in the presence of CO_2 contained in air. The above reveals that SGRCM has directly captured some carbon dioxide when exposed to air.

Figure 6c is the TG curve of SGRCM after 28 d hydration. As can be seen, after 28 d, the weight loss of SGRCM3 during the whole heating regime is the highest, indicating that more hydration products are formed in SGRCM3 compared with other groups. Figure 6d is the DTG curve of SGRCM after 28 d hydration. As can be seen, the endothermic peak of SGRCM3 at 100 °C is widest and sharpest. This suggests considering that SGRCM3 was the highest content of C-A-S-H and AFt under the activation of Na_2SiO_3, and correspondingly, the least Ca $(OH)_2$ was dehydrated at 450 °C. The obtained results thus indicate that in

the pozzolanic reaction activated by Na_2SiO_3, more $Ca(OH)_2$ crystals were converted to C-A-S-H gels [38,39]. Combined with results from microscopic analysis, one can see that C-A-S-H gel in SGRCM3 has filled the voids between AFt crystals, resulting in improved macroscopic mechanical properties shown by SGRCM3.

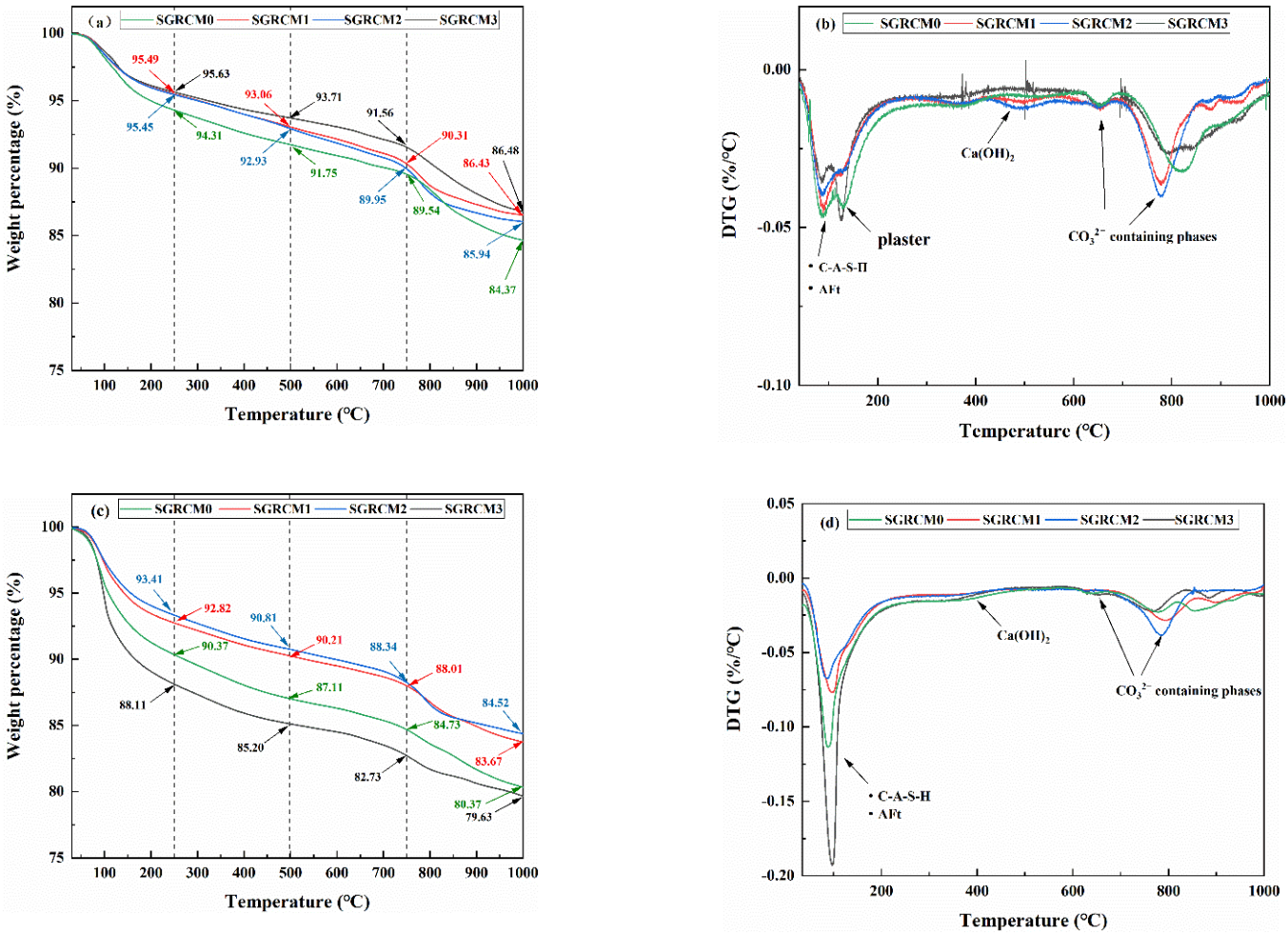


Figure 6. TGA/DTG curves of SGRCM under different activators for (**a**,**b**)1 d (**c**,**d**) 28 d.

3.5. SEM and EDS Analysis

Figures 7 and 8 depict the microscopic morphology of the hydration products of SGRCM0, SGRCM1, and SGRCM3 paste samples after 1 d and 28 d of curing. The amorphous network of the SGRCM0 paste sample was identified as a C-A-S-H gel using EDS analysis (Figure 7 region A). This network connected irregular hydration products of differing sizes in a loose manner [40]. Even though some unreacted particles were identified in local regions, the C-A-S-H gel covers the surface of these particles and fills the pores between particles of varying sizes forming a network structure that enhanced compressive strength. Needle-rod ettringite was detected in the C-A-S-H gel of the Na_2SiO_3-activated SGRCM3 sample.

The elemental composition of hydration products was determined using energy dispersive X-ray diffraction (EDS) analysis (Figure 7, areas A, B, and C). A single day of hydration leads to the formation of amorphous C-A-S-H gel in SGRCM0, SGRCM1, and SGRCM3 samples, analyzed by EDS. As the hydration process advanced, the Al^{3+}, K^+, and Na^+ in the sample were fixed in the hydration products. According to previous research, Al^{3+} might substitute Si^{4+} to bridge tetrahedral sites, generating a long chain structure of aluminum-containing C-A-S-H gel conducive to the development of compressive strength.

The net negative charge caused by substituting tetrahedral aluminum for silicon was balanced by other cations, such as K^+ and Na^+.

By comparison, C-A-S-H and ettringite were both produced under the activation of NaOH and Na_2SiO_3. Ettringite formed in Na_2SiO_3-activated samples was interlaced with C-A-S-H, and C-A-S-H also filled the ettringite's internal pores. In contrast, only ettringite was produced on the surface of SGRCM1 when the activation was done using NaOH, NaOH, and ettringite was neither dense nor compact. This explains the reason why its strength was very small.

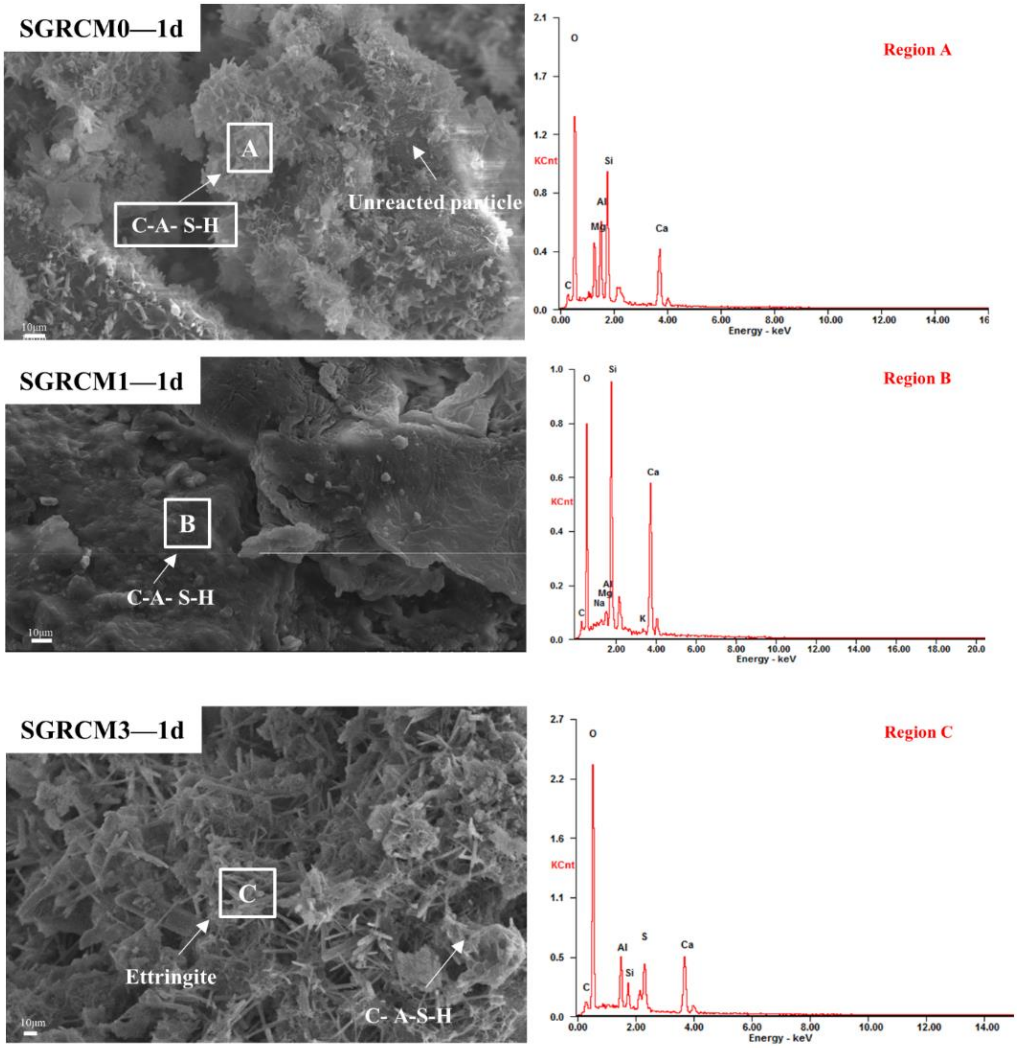


Figure 7. SEM images and EDS analysis of SGRCM0, SGRCM1, and SGRCM3 samples at 1 d.

As can be seen from SGRCM3-28d in Figure 7, the microstructure of the SGRCM slurry is dense, a thick amorphous C-A-S-H gel is observed, and the AFt is covered by the C-A-S-H gel. Rod-shaped AFt crystals and C-A-S-H gels are distributed in the holes and pits, which gradually grow and fuse, and the overall porosity of the material is greatly reduced. Therefore, the compactness of SGRCM3 is relatively high, and the macroscopic performance is high in mechanical properties.

The results of SEM and EDS analyses demonstrate once more that the principal hydration products of red mud, gold tailings, and ore powder were compound of amorphous C-A-S-H gel and fibrous ettringite crystals. As an activator, silicate enhanced the pozzolana activity of red mud and gold tailings, and promote the development of early strength. The activation effect of silicate was significantly superior to that of alkali and consistent with

some of their research [41,42]; thus, the geopolymer samples prepared in the present study were close to the typical normal geopolymer samples.

3.6. Ion Leaching Analysis

Raw material of slag, red mud, gold tailings, and SGRCM samples were leached using the sulfuric acid and nitric acid methods. Inductively coupled plasma mass spectrometry (ICP-MS) enabled ascertaining the toxicity of solutions from the leaching. Table 4 displays the concentrations and critical values of heavy metals in the leaching solution. After 28 dof curing, the concentration of heavy metal ions in SGRCM material revealed to comply with the HJ/T 299-2007 standard. As can be seen from Table 4, the concentration of all heavy metal ions in the leaching solution of sample SGRCM3 at 28 d were less than that at 1 d, showing the capacity of SGRCM3 to successfully solidify heavy metal ions. Crystals can solidify heavy metal ions because heavy metal ions can replace original ions in the crystal or enter voids in the crystal lattice [43]. The XRD pattern in Figure 4 has revealed that calcium-aluminite phases were present in hydration products. Figure 9 depicts the structural mechanism of anorthite formation. Typically, the basic structural unit of anorthite crystals is the tetrahedron, which is generated by the connection of four tetrahedrons and developed into three-dimensional space to form the basic framework. During hydration, Si-O tetrahedron is reorganized, and a portion of Si^{4+} in [SiO_4] tetrahedron can be replaced by Al^{3+} to produce [AlO_4] tetrahedron, producing a three-dimensional network structure consisting of [SiO_4] and [AlO_4] tetrahedron. The structure of this Al-Si frame is negatively charged. Consequently, the presence of heavy metal cations in the void of the frame contributes to the system's charge balance [44]. When heavy metal ions are included, due to the high bond strength of the calcium feldspar system, crystal nuclei are formed from the surrounding crystalline phases, and other heavy metal ions may be attracted to partially replace Si^{4+} or Al^{3+} ions to form similar [XO_4] tetrahedrons; this is a process that solidifies the heavy metal elements in the crystal lattice. Indeed, heavy metal ions can also replace calcium cations in anorthite crystal gaps [45]. Ca^{2+} ions in the anorthite phase can be substituted by Cu ions and Mg ions when heavy metal ions share the same ionic characteristics as calcium cations (e.g., the same positive bivalent charge) [46]. The above analysis demonstrates that heavy metal elements can be efficiently solidified in the SGRCM samples via two types of mechanisms: one is to substitute Si^{4+} or Al^{3+} ions in [SiO_4] or [AlO_4] tetrahedra to form [XO_4] tetrahedra (X is a heavy metal ion). The alternative is to replace Ca^{2+} in the interlayer and enter the network gap of the skeleton structure in order to counteract the negative charge. The cementitious materials prepared from red mud, waste gold tailings, and slag are therefore environmentally acceptable.

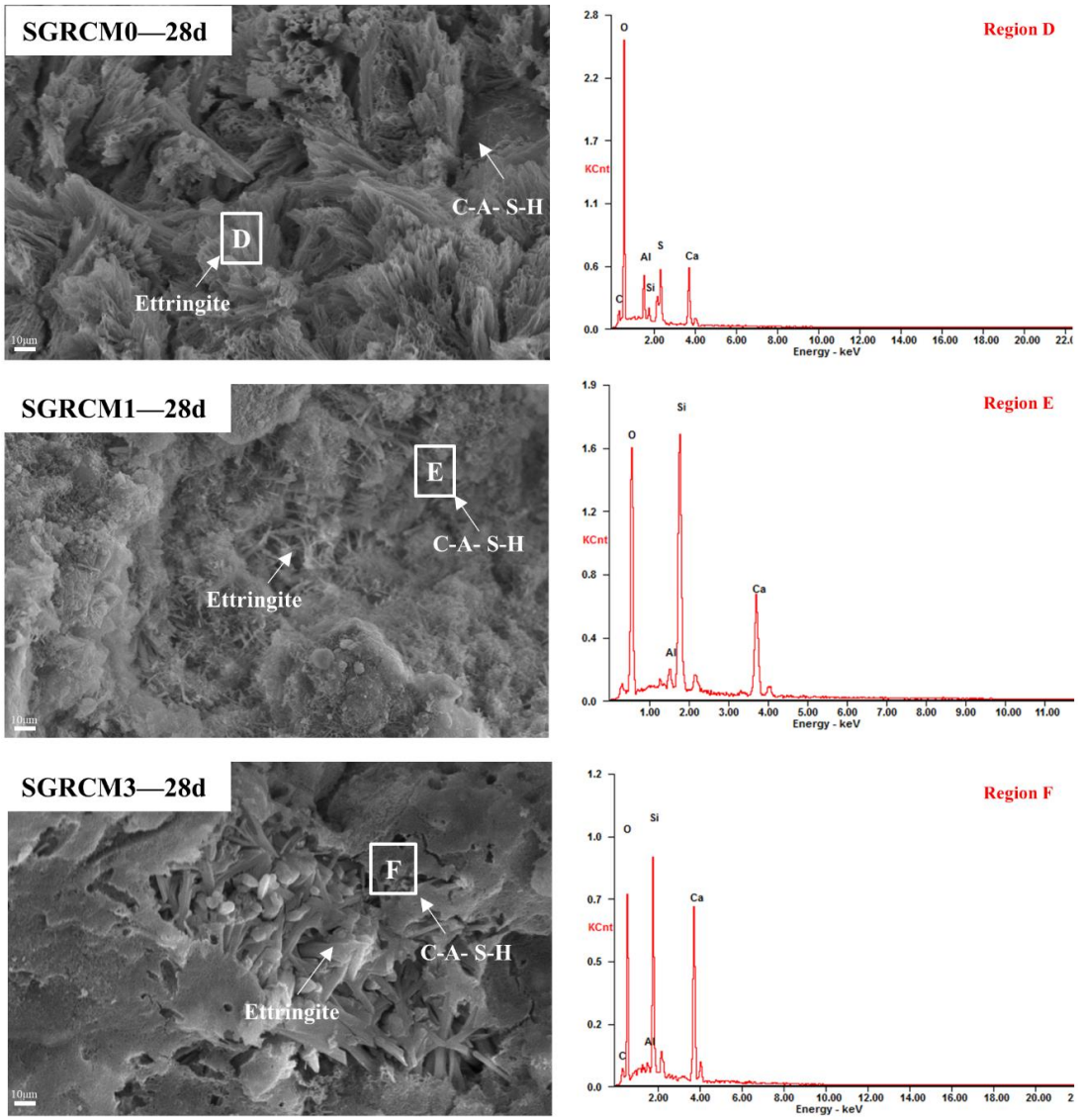


Figure 8. SEM images and EDS analysis of SGRCM0, SGRCM1, and SGRCM3 samples at 28 d.

Table 4. Leaching concentration of heavy metals in SGRCM with their critical limits.

Sample	Leaching Concentration of Heavy Metals				
	Al (mg/L)	As (mg/L)	Cu (mg/L)	Mo (mg/L)	Cr (mg/L)
SL	3.388	0	0	0.009	0
GT	0.053	0.080	0.005	0.016	0
RM	9.500	0.927	0.030	0.100	0.156
SGRCM0-1d	1.065	0.011	0.005	0.107	0.017
SGRCM1-1d	1.136	0.014	0.018	0.125	0.019
SGRCM2-1d	1.548	0.017	0.010	0.121	0.020
SGRCM3-1d	3.532	0.007	0.013	0.107	0.011
SGRCM0-28d	0.809	0.008	0.002	0.060	0.010
SGRCM1-28d	1.598	0.011	0.017	0.102	0.009
SGRCM2-28d	2.770	0.010	0.012	0.126	0.009
SGRCM3-28d	0.708	0	0.001	0.957	0.007
GB5085.3-2007critical limits	100	5	100	-	1

In SGRCM, the ion concentrations of Cd, Ag, Mn, Pb and Zn are all zero, so they are not listed.

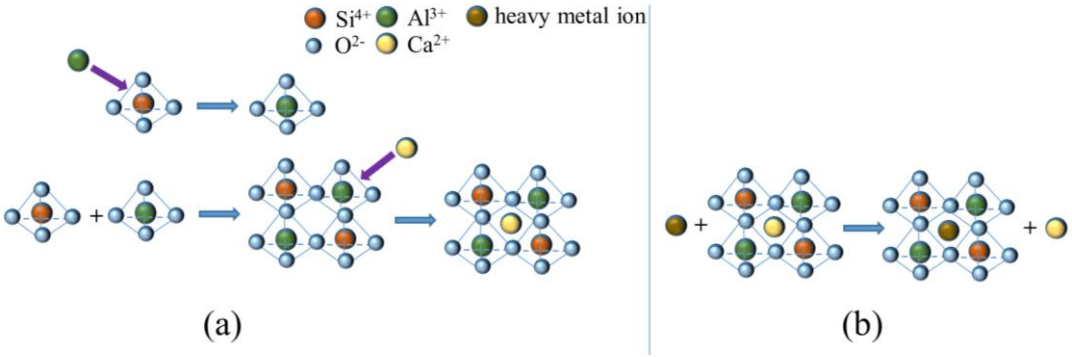


Figure 9. (**a**) The structural mechanism of anorthite formation, (**b**) the replacement of Ca by heavy metal ions.

4. Discussion and Conclusions

This paper attempts to use solid waste (red mud, gold tailings, and slag) instead of cement as a cementitious material in construction, providing a reference for future research on more green and environmentally friendly cementitious materials. In this study, the basic engineering indexes and environmental safety evaluation indexes of the specimens excited by different kinds of activators were tested. Meanwhile, the hydration products were characterized by XRD and FTIR. The main conclusions of this study are as follows:

1. The mass ratio of M (red mud) to M (gold tailings) to M (slag) to M (gypsum) in this study is 10:40:45:5. After curing at room temperature for 28 d, the compressive strength of SRCM3 reached 43.7 MPa.
2. According to XRD analyses, the hydration products of SGRCM3 are mainly composed of C-A-S-H and AFt, and this was in line with data from SEM and EDS analyses. Those hydration products are believed to have promoted the high compressive strength obtained.
3. The leaching concentrations of heavy metals in the samples were below the detection level, suggesting that the concentration of heavy metal ions in SGRCM were below the permitted limit for the environment. The obtained results indicate that the red mud-gold, tailing-slag, ternary composite cementitious material can consolidate heavy metal ions in a red mud.
4. The findings of the SRCM study indicate that the red-mud-gold-tailing-slag composite can be employed as a substitute for cement in industry when it is activated by Na_2SiO_3 (modulus = 1).

Author Contributions: Conceptualization, H.C. (Haonan Cui) and J.L.; methodology, H.C. (Haonan Cui) and T.H.; software, H.C. (Haonan Cui) and H.L.; validation, F.Y., H.C. (Haili Cheng) and H.L.; formal analysis, H.C. (Haili Cheng); investigation, J.L.; resources, T.H.; data curation, H.C. (Haonan Cui); writing—original draft preparation, H.C. (Haonan Cui); writing—review and editing, F.Y. and H.C. (Haili Cheng); visualization, H.C. (Haonan Cui); supervision, F.Y.; project administration, T.H. and F.Y.; funding acquisition, H.C. (Haili Cheng) All authors have read and agreed to the published version of the manuscript.

Funding: This research was funded by Beijing Building Materials Academy of Sciences Research, grant number 2021YFC1910605 and the APC was funded by School of Civil Engineering, North China University of Technology.

Institutional Review Board Statement: Not applicable.

Informed Consent Statement: Not applicable.

Data Availability Statement: Not applicable.

Acknowledgments: The authors are grateful for the support provided by the National Key R&D Program of China (2021YFC1910605), and Beijing Building Materials Academy of Sciences Research State key laboratory of solid waste resource utilization and energy saving building materials for the kind assistance in laboratory testing.

Conflicts of Interest: All authors disclosed no relevant relationships. The authors declared no potential conflicts of interest with respect to the research, authorship, and/or publication of this article.

References

1. Qi, Y. The neutralization and recycling of red mud—A review. *J. Phys. Conf. Ser.* **2021**, *1759*, 012004. [CrossRef]
2. Borra, C.R.; Blanpain, B.; Pontikes, Y.; Binnemans, K.; Van Gerven, T. Recovery of Rare Earths and Other Valuable Metals from Bauxite Residue (Red Mud): A Review. *J. Sustain. Metall.* **2016**, *2*, 365–386. [CrossRef]
3. Li, H.; Ye, H.; Zhu, J.; Liu, J. Research status of Bayer process red mud dealkalization technology. *J. Shandong Univ. Technol.* **2021**, *35*, 65–69.
4. Gräfe, M.; Power, G.; Klauber, C. Bauxite residue issues: III. Alkalinity and associated chemistry. *Hydrometallurgy* **2011**, *108*, 60–79. [CrossRef]
5. Ye, J.; Hu, A.; Ren, G.; Zhou, T.; Zhang, G.; Zhou, S. Red mud enhances methanogenesis with the simultaneous improvement of hydrolysis-acidification and electrical conductivity. *Bioresour. Technol.* **2018**, *247*, 131–137. [CrossRef] [PubMed]
6. Gelencser, A.; Kovats, N.; Turoczi, B.; Rostasi, A.; Hoffer, A.; Imre, K.; Nyiro-Kosa, I.; Csakberenyi-Malasics, D.; Toth, A.; Czitrovszky, A.; et al. The red mud accident in Ajka (Hungary): Characterization and potential health effects of fugitive dust. *Environ. Sci. Technol.* **2011**, *45*, 1608–1615. [CrossRef]
7. Ghalehnovi, M.; Roshan, N.; Hakak, E.; Shamsabadi, E.A.; de Brito, J. Effect of red mud (bauxite residue) as cement replacement on the properties of self-compacting concrete incorporating various fillers. *J. Clean. Prod.* **2019**, *240*, 118213. [CrossRef]
8. Senff, L.; Hotza, D.; Labrincha, J.A. Effect of red mud addition on the rheological behaviour and on hardened state characteristics of cement mortars. *Constr. Build. Mater.* **2011**, *25*, 163–170. [CrossRef]
9. Singh, B.; Ishwarya, G.; Gupta, M.; Bhattacharyya, S.K. Geopolymer concrete: A review of some recent developments. *Constr. Build. Mater.* **2015**, *85*, 78–90. [CrossRef]
10. Zhang, N.; Sun, H.; Liu, X.; Zhang, J. Early-age characteristics of red mud–coal gangue cementitious material. *J. Hazard. Mater.* **2009**, *167*, 927–932. [CrossRef]
11. Yao, G.; Liu, Q.; Wang, J.; Wu, P.; Lyu, X. Effect of mechanical grinding on pozzolanic activity and hydration properties of siliceous gold ore tailings. *J. Clean. Prod.* **2019**, *217*, 12–21. [CrossRef]
12. Dehghani, A.; Mostad-Rahimi, M.; Mojtahedzadeh, S.; Gharibi, K. Recovery of gold from the Mouteh Gold Mine tailings dam. *J. South. Afr. Inst. Min. Metall.* **2009**, *109*, 417–421.
13. Ndivhudzannyi, R.; Dacosta, F.; Gumbo, J. *Environmental Risk Assessment and Risk Management Strategies for Dysfunctional New Union Gold Mine in Malamulele, Limpopo, South Africa*; China University of Mining and Technology Press: Xuzhou, China, 2014.
14. Maroušek, J.; Stehel, V.; Vochozka, M.; Kolář, L.; Maroušková, A.; Strunecký, O.; Peterka, J.; Kopecký, M.; Shreedhar, S. Ferrous sludge from water clarification: Changes in waste management practices advisable. *J. Clean. Prod.* **2019**, *218*, 459–464. [CrossRef]
15. Rachman, R.; Bahri, A.; Trihadiningrum, Y. Stabilization and solidification of tailings from a traditional gold mine using Portland cement. *Environ. Eng. Res.* **2018**, *23*, 189–194. [CrossRef]
16. Kiventerä, J.; Golek, L.; Yliniemi, J.; Ferreira, V.; Deja, J.; Illikainen, M. Utilization of sulphidic tailings from gold mine as a raw material in geopolymerization. *Int. J. Miner. Process.* **2016**, *149*, 104–110. [CrossRef]
17. Consoli, N.C.; Nierwinski, H.P.; Peccin da Silva, A.; Sosnoski, J. Durability and strength of fiber-reinforced compacted gold tailings-cement blends. *Geotext. Geomembr.* **2017**, *45*, 98–102. [CrossRef]
18. Wu, Y.; Lu, B.; Bai, T.; Wang, H.; Du, F.; Zhang, Y.; Cai, L.; Jiang, C.; Wang, W. Geopolymer, green alkali activated cementitious material: Synthesis, applications and challenges. *Constr. Build. Mater.* **2019**, *224*, 930–949. [CrossRef]
19. Miranda, T.; Leitão, D.; Oliveira, J.; Corrêa-Silva, M.; Araújo, N.; Coelho, J.; Fernández-Jiménez, A.; Cristelo, N. Application of alkali-activated industrial wastes for the stabilisation of a full-scale (sub)base layer. *J. Clean. Prod.* **2020**, *242*, 118427. [CrossRef]
20. Tonini de Araújo, M.; Tonatto Ferrazzo, S.; Jordi Bruschi, G.J.; Consoli, N.C. Mechanical and Environmental Performance of Eggshell Lime for Expansive Soils Improvement. *Transp. Geotech.* **2021**, *31*, 100681. [CrossRef]
21. Acordi, J.; Luza, A.; Fabris, D.C.N.; Raupp-Pereira, F.; De Noni, A., Jr.; Montedo, O.R.K. New waste-based supplementary cementitious materials: Mortars and concrete formulations. *Constr. Build. Mater.* **2020**, *240*, 117877. [CrossRef]
22. Sithole, T.; Mashifana, T. Geosynthesis of building and construction materials through alkaline activation of granulated blast furnace slag-NC-ND license. *Constr. Build. Mater.* **2020**, *264*, 120712. [CrossRef]
23. Singh, S.; Aswath, M.U.; Ranganath, R.V. Effect of mechanical activation of red mud on the strength of geopolymer binder. *Constr. Build. Mater.* **2018**, *177*, 91–101. [CrossRef]
24. Wang, J.; Lyu, X.; Wang, L.; Cao, X.; Liu, Q.; Zang, H. Influence of the combination of calcium oxide and sodium carbonate on the hydration reactivity of alkali-activated slag binders. *J. Clean. Prod.* **2018**, *171*, 622–629. [CrossRef]
25. Ince, C. Reusing gold-mine tailings in cement mortars: Mechanical properties and socio-economic developments for the Lefke-Xeros area of Cyprus. *J. Clean. Prod.* **2019**, *238*, 117871. [CrossRef]

26. Jiang, H.; Qi, Z.; Yilmaz, E.; Han, J.; Qiu, J.; Dong, C. Effectiveness of alkali-activated slag as alternative binder on workability and early age compressive strength of cemented paste backfills. *Constr. Build. Mater.* **2019**, *218*, 689–700. [CrossRef]
27. Zhang, X.-F.; Ni, W.; Wu, J.-Y.; Zhu, L.-P. Hydration mechanism of a cementitious material prepared with Si-Mn slag. *Int. J. Miner. Metall. Mater.* **2011**, *18*, 234–239. [CrossRef]
28. Adesina, A.; Das, S. Influence of glass powder on the durability properties of engineered cementitious composites. *Constr. Build. Mater.* **2020**, *242*, 118199. [CrossRef]
29. Liu, X.; Zhang, N.; Sun, H.; Zhang, J.; Li, L. Structural investigation relating to the cementitious activity of bauxite residue—Red mud. *Cem. Concr. Res.* **2011**, *41*, 847–853. [CrossRef]
30. Cheah, C.B.; Tan, L.E.; Ramli, M. The engineering properties and microstructure of sodium carbonate activated fly ash/slag blended mortars with silica fume. *Compos. Part B Eng.* **2019**, *160*, 558–572. [CrossRef]
31. Somna, K.; Jaturapitakkul, C.; Kajitvichyanukul, P.; Chindaprasirt, P. NaOH-activated ground fly ash geopolymer cured at ambient temperature. *Fuel* **2011**, *90*, 2118–2124. [CrossRef]
32. Alonso, S.; Palomo, A. Alkaline activation of metakaolin and calcium hydroxide mixtures: Influence of temperature, activator concentration and solids ratio. *Mater. Lett.* **2001**, *47*, 55–62. [CrossRef]
33. Khale, D.; Chaudhary, R. Mechanism of geopolymerization and factors influencing its development: A review. *J. Mater. Sci.* **2007**, *42*, 729–746. [CrossRef]
34. Singh, P.S.; Bastow, T.; Trigg, M. Structural studies of geopolymers by 29Si and 27Al MAS-NMR. *J. Mater. Sci.* **2005**, *40*, 3951–3961. [CrossRef]
35. Mladenovič, A.; Mirtič, B.; Meden, A.; Zalar Serjun, V. Calcium aluminate rich secondary stainless steel slag as a supplementary cementitious material. *Constr. Build. Mater.* **2016**, *116*, 216–225. [CrossRef]
36. Chen, H.; Yuan, H.; Mao, L.; Hashmi, M.Z.; Xu, F.; Tang, X. Stabilization/solidification of chromium-bearing electroplating sludge with alkali-activated slag binders. *Chemosphere* **2020**, *240*, 124885. [CrossRef]
37. Collier, N.C. Transition and Decomposition Temperatures of Cement Phases—A Collection of Thermal Analysis Data. *Ceram. Silik.* **2016**, *60*, 338–343. [CrossRef]
38. Rashad, A.M.; Zeedan, S.R.; Hassan, A.A. Influence of the activator concentration of sodium silicate on the thermal properties of alkali-activated slag pastes. *Constr. Build. Mater.* **2016**, *102*, 811–820. [CrossRef]
39. Wan, Q.; Rao, F.; Song, S.; García, R.E.; Estrella, R.M.; Patiño, C.L.; Zhang, Y. Geopolymerization reaction, microstructure and simulation of metakaolin-based geopolymers at extended Si/Al ratios. *Cem. Concr. Compos.* **2017**, *79*, 45–52. [CrossRef]
40. Li, H.; Guan, X.; Zhang, X.; Ge, P.; Hu, X.; Zou, D. Influence of superfine ettringite on the properties of sulphoaluminate cement-based grouting materials. *Constr. Build. Mater.* **2018**, *166*, 723–731. [CrossRef]
41. Guo, X.; Zhang, L.; Huang, J.; Shi, H. Detoxification and solidification of heavy metal of chromium using fly ash-based geopolymer with chemical agents. *Constr. Build. Mater.* **2017**, *151*, 394–404. [CrossRef]
42. Nath, S.K.; Kumar, S. Reaction kinetics, microstructure and strength behavior of alkali activated silico-manganese (SiMn) slag –Fly ash blends. *Constr. Build. Mater.* **2017**, *147*, 371–379. [CrossRef]
43. Cheng, X.; Long, D.; Zhang, C.; Gao, X.; Yu, Y.; Mei, K.; Zhang, C.; Guo, X.; Chen, Z. Utilization of red mud, slag and waste drilling fluid for the synthesis of slag-red mud cementitious material. *J. Clean. Prod.* **2019**, *238*, 117902. [CrossRef]
44. Huang, Z.; Liu, K.; Duan, J.; Wang, Q. A review of waste-containing building materials: Characterization of the heavy metal. *Constr. Build. Mater.* **2021**, *309*, 125107. [CrossRef]
45. Lee, W.K.W.; van Deventer, J.S.J. The effect of ionic contaminants on the early-age properties of alkali-activated fly ash-based cements. *Cem. Concr. Res.* **2002**, *32*, 577–584. [CrossRef]
46. Yunsheng, Z.; Wei, S.; Qianli, C.; Lin, C. Synthesis and heavy metal immobilization behaviors of slag based geopolymer. *J. Hazard. Mater.* **2007**, *143*, 206–213. [CrossRef]